

# Fabrication of Gamma-Ray Shielding Using Rapid Breakdown Anodization

H. HAKIM, A.N. MOHAMMED AND M.S. HASHIM\*

*Physics Department, Education College, Mustansiriyah University, 14022 Baghdad, Iraq*

Received: 11.07.2023 & Accepted: 07.09.2023

Doi: [10.12693/APhysPolA.144.255](https://doi.org/10.12693/APhysPolA.144.255)

\*e-mail: [mustmust@uomustansiriyah.edu.iq](mailto:mustmust@uomustansiriyah.edu.iq)

The rapid breakdown anodizing method was used to produce (Bi, Bi<sub>2</sub>O<sub>3</sub>), (Pb, PbO<sub>2</sub>), and WO<sub>3</sub> nanoparticles. These particles are utilized to fabricate gamma-ray shielding. The X-ray diffraction test displayed polycrystalline structures for all samples. Scanning electron microscope images illustrated the formation of (Bi, Bi<sub>2</sub>O<sub>3</sub>) and (Pb, PbO<sub>2</sub>) nanoplates and WO<sub>3</sub> semi-sphere particles. Pressures of 318, 477, and 636 MPa were applied to reduce vacancies within the prepared powders and increase their densities. Cylindrical samples with a diameter of 14 mm and different thicknesses were formed. Utilizing gamma rays produced by sources like Am-241 (59.54 keV), Cs-137 (661.6 keV), Co-60 (1173 keV), and Co-60 (1332 keV), the shielding characteristics of the manufactured samples were studied. The linear attenuation coefficient, mass attenuation coefficient, and half-value layer were determined after the gamma flux was measured using a NaI(Tl) detector. The two attenuation coefficients were functions of the source energy, and they had the highest values for (Pb, PbO<sub>2</sub>) and the lowest for the WO<sub>3</sub> sample. The atomic numbers of the elements used and the size of the voids inside the prepared powders played the greatest role in determining the values of the shielding parameters.

topics: shielding, gamma ray, anodization, nanoparticles

## 1. Introduction

The number of useful applications of various radiations in industry, agriculture, research, and medicine, as well as for nuclear power production, is growing daily as a result of the advancement of nuclear technology throughout time. However, a disadvantage to these peaceful applications of radiation is that they may have a negative impact on nearby workers if exposure exceeds the allowable dose level. When radiation penetrates organs or tissues, it loses some of its energy through various interactions. This energy loss may ionize the atoms of the cell, causing the cell's natural chemical balance to be destroyed and ultimately leading to cell death. As a result, the radiation needs to be sufficiently attenuated to protect workers from its negative effects while still allowing them to perform their work [1].

The most effective gamma radiation absorbers are dense materials made of heavy atoms, such as lead, bismuth, and tungsten. However, because of its high density, high atomic number, and low cost, lead is a superior material to other shielding materials despite its poisonous nature and poor mechanical qualities. As a result, numerous significant disadvantages restrict its applications and uses. To replace outdated radiation shielding materials like lead, it is therefore vital to look for new radiation shielding materials [2].

When compared to traditional shielding members that use micro-particles, radiation shielding members with nanoparticles as the shielding material further increase the collision probability of the shielding material with radiation. This decreases the mean free path of radiation in the shielding member, resulting in superior radiation shielding effects [3]. There are reports of the use of several nanomaterials and nanocomposites in the radiation shielding of various ionizing energies. Therefore, the investigation of gamma radiation shielding utilizing various materials has been the major subject of numerous research publications [4]. Sttar et al. [5] reported that the values of the linear attenuation coefficient (*LAC*) for nanoparticles were higher than those for micromaterials. Additionally, their results indicate that the half-value layer (*HVL*) and dosage rate are lower than they would be for nanoparticles [5].

Various methods have been used to synthesize nanomaterials used for shielding against gamma rays. Rashad et al. [6] used the solid-solid reaction method to create MgO and ZnO nanoparticles and investigated the nuclear radiation shielding properties of these nanoparticles. The low-temperature solution combustion method was utilized by Reddy et al. [7] to produce Bi<sub>2</sub>O<sub>3</sub> nanoparticles and study their X-ray and gamma-ray radiation shielding properties.

In the current contribution, to prepare nanomaterials, the rapid breakdown anodization (RBA) technique was used, which is a simple, cheap, uncomplicated, and relatively fast method. This method transfers the metal to its oxide with the same element's nanoparticles. Using the RBA approach, nanooxides were created for a variety of applications, including photocatalytic decolorization, sensors, and bioactive materials [8–10]. This technique offers a straightforward way to create various nanooxides that are deposited on different bases and have diverse shapes and compositions. Hashim et al. [11] generated nanoparticles using this process as precipitated powders of several minerals, including ZnO, Cu<sub>2</sub>O, MgO, and TiO<sub>2</sub>. To the best of our knowledge, there is no paper dealing with the preparation of nanomaterials by RBA for gamma shielding.

The aim of this work is to prepare active gamma shielding materials using the RBA technique.

## 2. Experimental part

### 2.1. Preparation of nanomaterials by rapid breakdown anodization

Three powders of (Bi, Bi<sub>2</sub>O<sub>3</sub>), (Pb, PbO<sub>2</sub>), and (WO<sub>3</sub>) were prepared by RBA technique using the following procedure: After cleaning with alcohol, (Pb, Fe, or W) foils (0.1 mm thick) with

a rectangular shape ( $1 \times 2 \text{ cm}^2$ ) were immersed in 0.1 M HClO<sub>4</sub> electrolyte. In the anodization process, two pieces of the same materials were used — one as a working electrode and the other as a counter. The distance between the two electrodes was 0.5 cm, and the applied voltage between them was 20 V. The anodic process took an hour. In this period, the used foil was transformed completely into powder, and then the wet powder was dried on a hot plate.

### 2.2. Preparation of compressed samples

Tables I–III show the weights and thicknesses of the samples and the pressure to which they were subjected. The shape of all samples is cylindrical, with a diameter of 14 mm.

### 2.3. Characterization of the produced powders

To establish the materials' crystalline nature, a powder X-ray diffractometer (Shimadzu, Japan) was utilized. The topographies of the surfaces and the sizes of the generated particles were determined using the scanning electron microscopy (SEM) method. The system used was one of the German Carl Zeiss's models; the same system was used to test energy dispersive X-ray spectroscopy (EDX) of prepared samples.

TABLE I

Weights, thicknesses, and densities of the compressed (Pb, PbO<sub>2</sub>) samples.

(group 1)			(group 2)			(group 3)		
Pressure of 318 MPa			Pressure of 477 MPa			Pressure of 636 MPa		
Weight [g]	Thickness [mm]	Density [g/cm <sup>3</sup> ]	Weight [g]	Thickness [mm]	Density [g/cm <sup>3</sup> ]	Weight [g]	Thickness [mm]	Density [g/cm <sup>3</sup> ]
1.5	1.41	6.91	1.5	1.23	7.92	1.5	1.16	8.40
2	2.1	6.18	2	1.78	7.30	2	1.56	8.33
2.5	2.91	5.58	2.5	2.69	6.04	2.5	2.77	5.86
3.5	3.51	6.48	3.5	3.01	7.55	3.5	2.99	7.60
4	4.32	6.01	4	3.92	6.63	4	3.93	6.61

TABLE II

Weights, thicknesses, and densities of the compressed WO<sub>3</sub> samples.

(group 1)			(group 2)			(group 3)		
Pressure of 318 MPa			Pressure of 477 MPa			Pressure of 636 MPa		
Weight [g]	Thickness [mm]	Density [g/cm <sup>3</sup> ]	Weight [g]	Thickness [mm]	Density [g/cm <sup>3</sup> ]	Weight [g]	Thickness [mm]	Density [g/cm <sup>3</sup> ]
1	1.91	3.40	1	1.7	3.82	1	1.53	4.24
1.5	2.52	3.86	1.5	2.23	4.37	1.5	2.22	4.39
2	3.10	4.19	2	2.84	4.57	2	2.73	4.76
2.5	4.43	3.66	2.5	3.85	4.22	2.5	3.65	4.45
3.5	5.62	4.04	3.5	5.46	4.16	3.5	5.26	4.32

TABLE III

Weights, thicknesses, and densities of the compressed (Bi, Bi<sub>2</sub>O<sub>3</sub>) samples.

(group 1)			(group 2)			(group 3)		
Pressure of 318 MPa			Pressure of 477 MPa			Pressure of 636 MPa		
Weight [g]	Thickness [mm]	Density [g/cm <sup>3</sup> ]	Weight [g]	Thickness [mm]	Density [g/cm <sup>3</sup> ]	Weight [g]	Thickness [mm]	Density [g/cm <sup>3</sup> ]
2	2.31	5.62	2	2.12	6.13	2	1.94	6.70
2.5	2.92	5.56	2.5	2.6	6.25	2.5	2.15	7.55
3	3.26	5.98	3	3.00	6.5	3	2.82	6.91
3.5	3.62	6.28	3.5	3.38	6.73	3.5	3.03	7.50
4.5	4.97	5.88	4.5	4.66	6.27	4.5	4.40	6.64
5	6.30	5.15	5	5.12	6.34	5	4.76	6.82

#### 2.4. Characterization of shielding properties

Four radioactive sources, Am-241 (59.54 keV), Cs-137 (661.6 keV), Co-60 (1173 keV), and Co-60 (1332 keV) and an HPGe detector were used. The counting rate was calculated using a program connected to the device (Genie 2000 program). The counting rate  $I$  for each sample was calculated, then the sample was removed and the free counting rate was calculated ( $I_0$ ).

The following formula was used to determine the  $LAC$  from the count rate calculation [12]

$$LAC = \frac{1}{x} \frac{I_0}{I}, \quad (1)$$

where  $x$  is the thickness of the sample. Material thickness sufficient to reduce the gamma-ray intensity by 50% is  $HVL$ . Utilizing the following equation,  $HVL$  is determined [13]

$$HVL = \frac{\ln(2)}{LAC}. \quad (2)$$

The mass attenuation coefficient ( $MAC$ ) of the sample is estimated using the equation [7]

$$MAC = \frac{LAC}{\rho}, \quad (3)$$

where  $\rho$  is the density of the sample.

Model NAIS, a sodium iodide scintillation detector with high efficiency, was used. The system contains a NaI(Tl) crystal in an aluminum housing, a photomultiplier tube, an internal magnetic or light shield, a high-voltage power supply (HVPS), stabilization electronics, a preamplifier, and an 8-pin Mirion proprietary connector.

WinXCom software (the Windows version of XCOM, a well-known program for calculating X-ray and gamma-ray attenuation coefficients and interaction cross sections) was used to calculate the  $MAC$  values of the three compressed samples. Calculating  $MAC$  values with this XCOM software includes giving the exact percentage of each of the components that make up the shielding. In the case of (Pb, PbO<sub>2</sub>) samples, for example, the percentage of lead, lead oxide, and components of the air that fill the spaces in each sample were included.

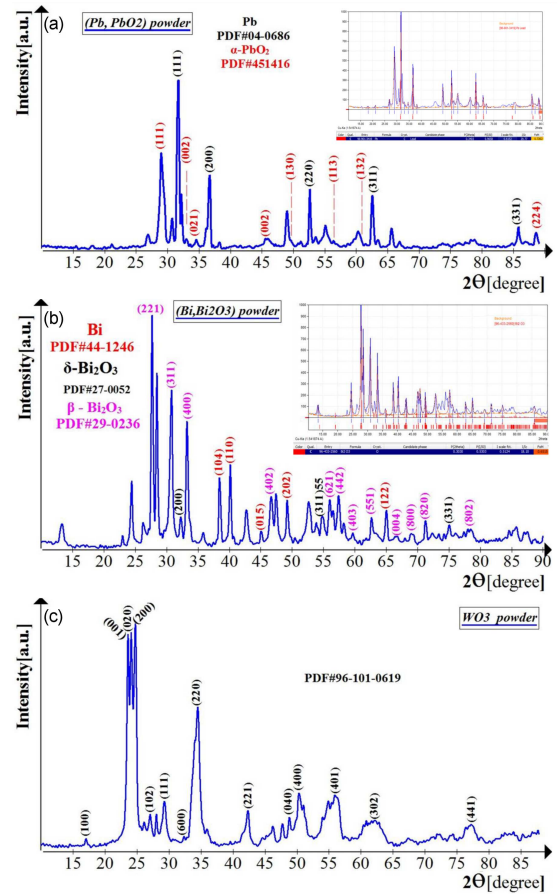


Fig. 1. XRD pattern of (a) (Pb, PbO<sub>2</sub>) powder, (b) (Bi, Bi<sub>2</sub>O<sub>3</sub>) powder, and (c) WO<sub>3</sub> powder. Inset — XRD pattern with components ratios using Match software.

### 3. Results and discussion

#### 3.1. Materials characterization

The structural features of the prepared powders were studied using the X-ray diffraction (XRD) technique. The patterns (intensity of diffracted X-rays as a function of  $2\theta$ ) of these powders are shown in Fig. 1, where  $\theta$  is the diffraction angle.

TABLE IV

EDX compositions of the three compressed samples.

(Pb, PbO <sub>2</sub> )				(Bi, Bi <sub>2</sub> O <sub>3</sub> )				WO <sub>3</sub>			
Element	Intensity	wt%	at.%	Element	Intensity	wt%	at.%	Element	Intensity	wt%	at.%
C	95.6	4.40	20.8	O	290.6	19.35	60.45	C	49.7	6.12	14.23
O	234.7	16.1	57.3	Bi	4200.1	75.49	18.06	O	410.8	44.86	78.32
Pb	4384.4	79.4	21.8	C	130.8	5.16	21.49	W	718.3	49.02	7.45

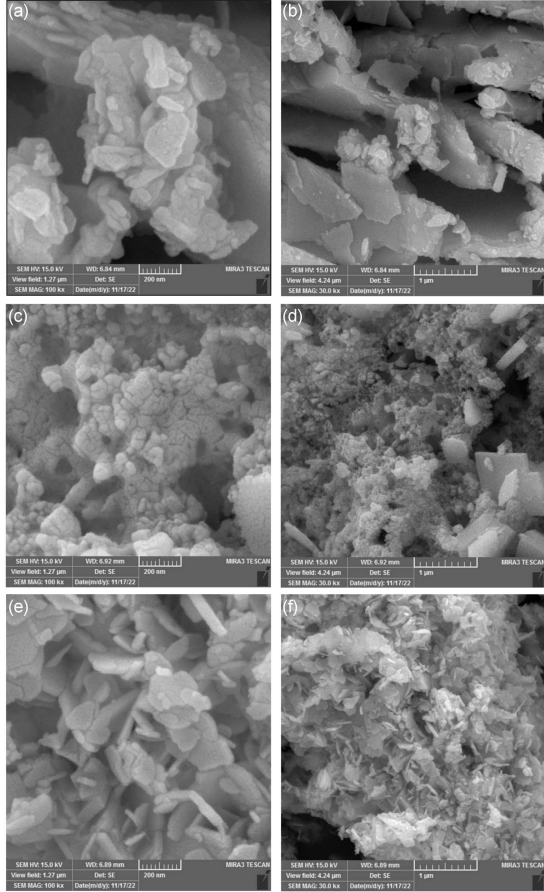


Fig. 2. Scanning electron microscope (SEM) images of (a, b) (Pb, PbO<sub>2</sub>) powder, (c, d) (Bi, Bi<sub>2</sub>O<sub>3</sub>) powder, and (e, f) (WO<sub>3</sub>) powder.

In the XRD pattern of (Pb, PbO<sub>2</sub>) powder (Fig. 1a), there are five peaks (111), (200), (220), (311), and (331) due to Pb, and the rest of the peaks are due to PbO<sub>2</sub>. This shows that the anodizing process did not completely convert the lead element into its oxide and that the powder contains a number of lead nanoparticles associated with lead oxide nanoparticles. This result is in agreement with that obtained by Hashim et al. [10], who prepared by the RBA technique several oxides mixed with nanoparticles of the element used for preparation. Match software was used to calculate the ratio of each part in (Pb, PbO<sub>2</sub>) powder; the ratios were 72 and 28% for Pb and PbO<sub>2</sub>, respectively; see the inset in Fig. 1a.

The XRD pattern of (Bi<sub>2</sub>O<sub>3</sub>) powder (Fig. 1b)

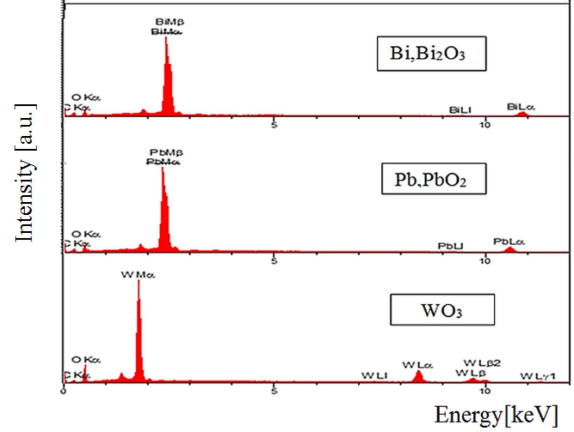


Fig. 3. EDX spectra for the produced powders.

confirms the transformation of bismuth metal into bismuth oxide in two phases ( $\delta$ -Bi<sub>2</sub>O<sub>3</sub> and  $\beta$ -Bi<sub>2</sub>O<sub>3</sub>), with the remaining percentage of unconverted Bi element equal to 35%. According to Match! software, the ratio of Bi oxide inside the sample is 65%; see the inset in Fig. 1b.

Figure 1c shows the complete conversion of W to WO<sub>3</sub>. The dominant characteristic of the three XRD patterns in Fig. 1 is that they are all polycrystalline and highly crystalline and that the dominant peaks in the two patterns of (Bi, Bi<sub>2</sub>O<sub>3</sub>) and WO<sub>3</sub> powders are due to oxides, but in the diffraction pattern of (Pb, PbO<sub>2</sub>), the dominant peak belongs to the element and not to the oxide.

Figure 2 shows SEM images of the three powders.

EDX spectra are illustrated in Fig. 3, the peaks of elements are dominant, and there is a peak for the existence of oxygen.

Table IV shows that all the elements used are oxidized, but in different proportions.

TABLE V

The volume of air [cm<sup>3</sup>] inside one gramm of each sample before and after pressure.

Powder type	Pressure [MPa]			
	As prepared	318	477	636
(Pb+PbO <sub>2</sub> )	0.29	0.0486	0.0316	0.0236
(Bi+Bi <sub>2</sub> O <sub>3</sub> )	0.724	0.0663	0.0573	0.0443
WO <sub>3</sub>	0.86	0.155	0.1226	0.0965

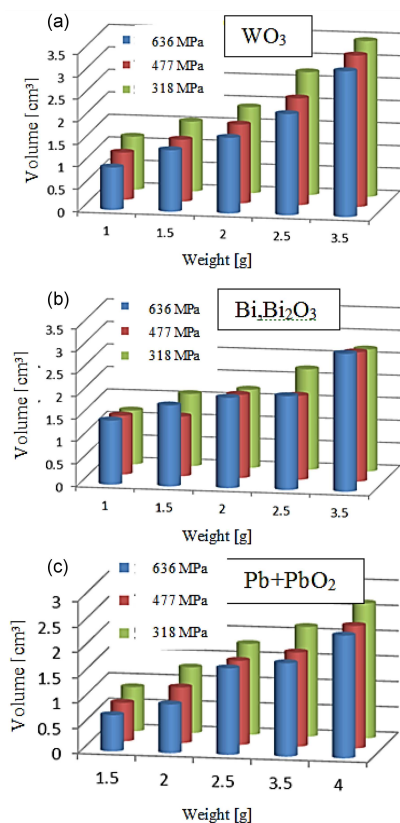


Fig. 4. Volume versus weight for variable pressures.

Voids can be observed in all powders. The (Pb, PbO<sub>2</sub>) and WO<sub>3</sub> powders consist of nanosheets (see Fig. 2a, b), while the (Bi, Bi<sub>2</sub>O<sub>3</sub>) powder consists of irregular nanoparticles (see Fig. 2c). Asgari et al. [2] reported that more attenuation was attained when the particle diameters were in the nanoscale order. However, particle size did not significantly contribute to improved attenuated photon flux at higher energies. The possibility of a collision between incoming gamma rays and nano-size materials appears to rise with decreasing particle size and homogenous dispersion of nanoparticles [2]. The qualities of the shielding member are negatively impacted by the existence of vacancies, and the radiation shielding effects are prevented from improving. The radiation-shielding materials should thus have porosity as low as practicable. So, in this work, the application of pressure to all powders is the direct way to minimize the vacancies. The volumes of spaces inside one gram of each sample before and after pressure are calculated and are listed in Table V.

It is noticeable in Table V that for all samples, the voids decreased with pressure, but the largest decrease was when 10 tons were applied to the powders. Larger voids were permeated with WO<sub>3</sub> powder, and the smaller ones with (Pb + PbO<sub>2</sub>) powder.

Figure 4 shows the variation of samples' volumes

with their weight; it is clear that volume decreases with pressure, however, at a different rate. This behavior has a direct effect on shielding properties, which will be clarified in the following paragraphs.

The volume of each powder is the volume of the material plus the volume of air inside the powder. It is clear from Table VI that the powder with a higher density has a smaller volume and fewer spaces inside it.

### 3.2. Radiation shielding properties of the compressed powders

A portion of the incident photons is completely absorbed, while the remaining photons transmit their full energy. In general, the gamma rays incident on an absorber material may either absorb or scatter in a single event through various interaction processes with the different components of the absorber. The interaction cross sections and probabilities resulting from each composite component are added to get the total linear attenuation coefficient. Material density directly affects interaction probability and, as a result, the linear attenuation coefficient [14].

For the three powders, *LACs* were calculated and tabulated in Table VII, and also shown in Fig. 5. The results present an increasing trend in *LAC*, with the pressure increasing for three tested samples. For a certain mass of material, increasing the pressure reduces the thickness, increases the density, and increases the *LAC*. For effective shielding of larger energies, it needs higher materials' densities (higher pressure).

These results confirm that increasing pressure can lead to a remarkable improvement in gamma-ray shielding. The maximum *LAC* values were recorded for (Pb, PO<sub>2</sub>) powder for all tested energies. This result is a direct outcome of the high density values of both Pb and PO<sub>2</sub> compared with those of (WO<sub>3</sub>) and (Bi, Bi<sub>2</sub>O<sub>3</sub>) powders; see Table VI. Also, the spaces' volumes inside the (Pb, PO<sub>2</sub>) powders are smaller than those for the rest of the powders; see Table V.

It was expected that *LAC* of (Bi, Bi<sub>2</sub>O<sub>3</sub>) powder would be greater than that of (Pb, PO<sub>2</sub>), given that bismuth's atomic number is greater, but the low ratio of bismuth to its oxide inside its powder decreases its shielding properties. On the other hand, the ratio of lead to its oxide inside its powder is the reason behind the relatively high *LAC* of (Pb, PO<sub>2</sub>) powder; see Fig. 5.

The *LAC* values for (Bi, Bi<sub>2</sub>O<sub>3</sub>) are higher than those for (WO<sub>3</sub>), as shown in Table VI. It can be attributed to the larger values of densities for (Bi, Bi<sub>2</sub>O<sub>3</sub>) compared to those for (WO<sub>3</sub>); see Tables II and III. Also, the volume of air inside WO<sub>3</sub> powder is larger than that for (Bi, Bi<sub>2</sub>O<sub>3</sub>) powder after pressure; see Table IV. The increase in volume of the material with the increase in mass includes an

TABLE VI

Some physical properties of as prepared samples.

	WO <sub>3</sub>	(Bi, Bi <sub>2</sub> O <sub>3</sub> )	(Pb, PbO <sub>2</sub> )
Powder density	1 g/cm <sup>3</sup>	1.2 g/cm <sup>3</sup>	2.06 g/cm <sup>3</sup>
Powder volume of 1 g	1 cm <sup>3</sup>	0.833 cm <sup>3</sup>	0.484 cm <sup>3</sup>
Element standard density	$\rho_W = 19.3 \text{ g/cm}^3$	$\rho_{Bi} = 9.78 \text{ g/cm}^3$	$\rho_{Pb} = 11.34 \text{ g/cm}^3$
Oxide standard density	$\rho_{WO_3} = 7.16 \text{ g/cm}^3$	$\rho_{Bi_2O_3} = 8.9 \text{ g/cm}^3$	$\rho_{PbO_2} = 9.38 \text{ g/cm}^3$
Atomic number	$Z_W = 74$	$Z_{Bi} = 83$	$Z_{Pb} = 82$

TABLE VII

LAC for the three prepared powders.

Powder	Pressure [MPa]	Am-241 with 59.54 keV	Cs-137 with 661.6 keV	Co-60 with 1173 keV	Co-60 with 1332 keV
(Pb,PO <sub>2</sub> )	318	2.98	1.39	1.01	1.11
	477	3.08	1.46	1.08	1.12
	1.13	1.23	1.48	3.25	636
(Bi,Bi <sub>2</sub> O <sub>3</sub> )	0.819	0.756	1.283	2.103	318
	0.911	0.848	1.413	2.255	477
	0.935	0.874	1.419	2.673	636
WO <sub>3</sub>	0.699	0.671	1.114	2.133	318
	0.770	0.69	1.169	2.175	477
	0.905	0.738	1.186	2.360	636

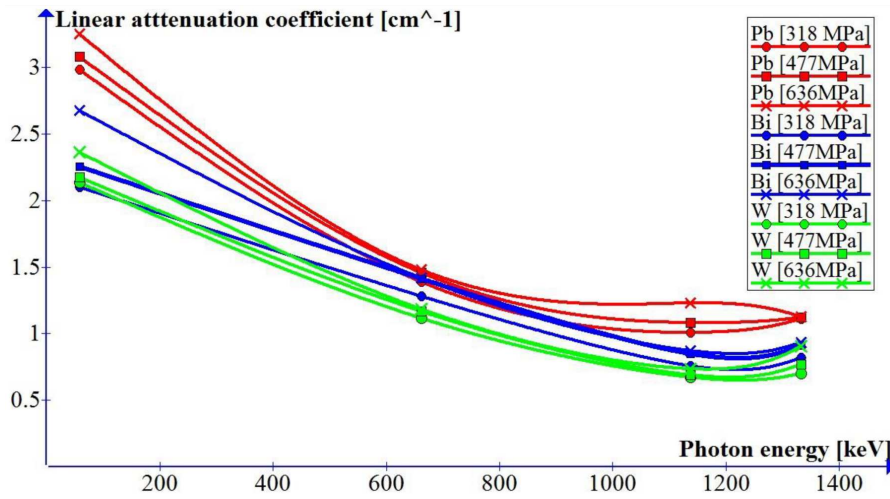


Fig. 5. LAC as a function of photon energy for different pressures .

increase in the air spaces penetrated inside the material. The increase in pressure decreased the volume of powder, decreasing the vacancies inside it. As a result, LAC increased with decreasing air vacancies (increasing pressure).

High-atomic-number elements, which are more effective in attenuating gamma rays, are what cause the highest MAC. The three ways in which gamma rays interact with materials are the photoelectric effect, pair creation, and the Compton effect. The occurrence of Compton scattering is directly proportional to the atomic number ( $Z$ ) of

the material, and it is common at medium energies (0.662–1.25 MeV) [16]. WO<sub>3</sub> powder has the highest MAC across the low energy range; see Fig. 6.

In Fig. 6, it can be seen that MAC decreases as photon energy rises (along with the photoelectric effect), and when photon energy exceeds 1250 keV, MAC of all shielding materials roughly equals itself over a specific energy range. The reason is that all elements on which MAC depends have an atomic number to atomic weight ratio ( $Z/M$ ) that is roughly equal to 12, with the exception of hydrogen and the heavy elements, at this intermediate energy

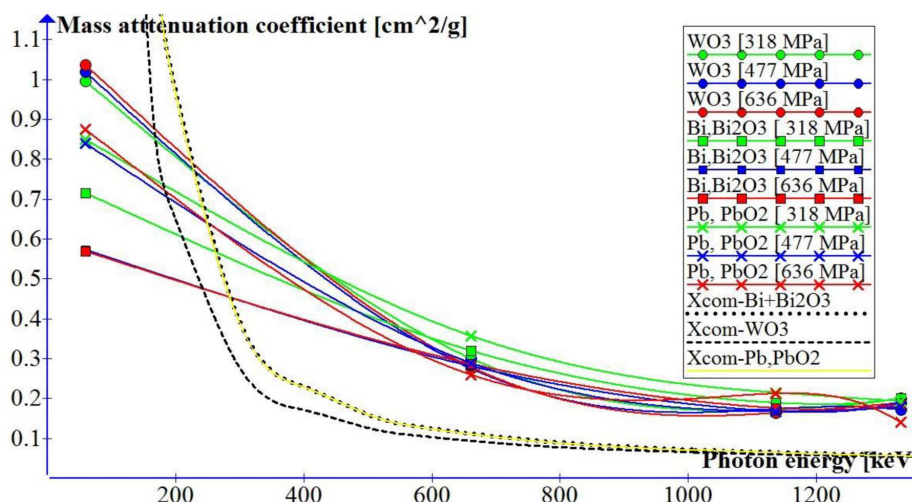


Fig. 6. Theoretical and practical relationships between *MAC* and photon energy.

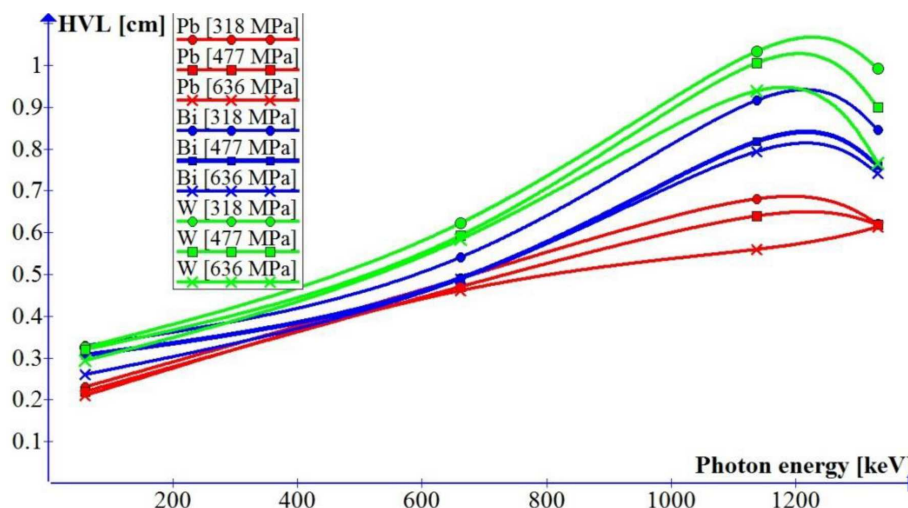


Fig. 7. *HVL* as a function of photon energy.

range where Compton scattering predominates [1]. As the energy range in the Compton scattering region rises, the reduction of *MAC* is proportional to  $E^{-1}$  [17].

The calculated values (theoretical values) for the samples are plotted in Fig. 6 under the respective labels Xcom-Bi + Bi<sub>2</sub>O<sub>3</sub>, Xcom-WO<sub>3</sub>, and Xcom-Pb,PbO<sub>2</sub>. For all samples, after comparison with the theoretical values, it is clear that the *MAC* values for compressed samples are improved after 300 keV. The difference between the practical and theoretical values in the behavior of changing the mass attenuation coefficient (*MAC*) between 60 and 300 keV is clear, as the rate of decrease for the theoretical values is faster than that for the practical values. It can also be noted that the behavior of the theoretical (Bi, Bi<sub>2</sub>O<sub>3</sub>) curve converges with that of (Pb, PbO<sub>2</sub>) and their relative divergence in the practical curves in the region confined between 60 and 300 keV.

It is useful to mention that the XCOM database does not take into account solid-state and molecular effects. Only single isolated neutral atoms are included in the element cross sections. Inconsistencies between experimental and XCOM results for complicated composite architectures may thus exist [18].

*HVL* is an essential variable when constructing any radiation shielding since it specifies the thickness of an absorber that must be used to bring the radiation level down to its initial value. The computed *HVL* of the sample materials for the specified source energy is depicted in Fig. 7. The gamma-ray penetration power of the incoming photon, which rises with increasing energy, is correlated with the increase in the *HVL* with increasing energy. As a result, when the penetration power grows, the transmission factor ( $I_0/I$ ) rises as well, increasing the thickness needed to attenuate half of the incident photons [15].

The *HVL* data in Fig. 7 showed a significant decrease in *HVL* with pressure of all samples.

The gamma-ray penetration strength of the incoming photon, which rises with increasing energy, correlates with the increase in *HVL* with increasing energy.

#### 4. Conclusions

The RBA method is an appropriate technique for producing nanoparticles that are effective at attenuating gamma rays.

- The pressure process is necessary and essential to reduce the voids inside the prepared powders and obtain effective shielding materials from RBA.
- Overcoming voids within nanopowders is necessary even for elements with high atomic numbers, such as bismuth or lead.
- Measured *MAC* in practice differs from theoretical predictions, which may be due to effects not accounted for by the mathematical model of XCOM software.

#### Acknowledgments

The authors are grateful for the support provided by the Directorate of Central Laboratories in the Iraqi Atomic Energy Commission, Baghdad, Iraq. The authors are also grateful to the Mustansiriyah University management for their support.

#### References

- [1] R. Biswas, H. Sahadath, A.S. Mollah, M. Fazlul Huq, *J. Radiat. Res. Appl. Sci.* **9**, 26 (2016).
- [2] M. Asgari, H. Afarideh, H. Ghafoorifard, E.A. Amirabadi, *Nucl. Eng. Technol.* **53**, 4142 (2021).
- [3] M.I. Sayyed, H. Al-Ghamdi, A.H. Almuqrin, S. Yasmin, M. Elsafi, *Polymers* **14**, 2867, (2022).
- [4] E.A. Allam, R.M. El-Sharkawy, A. El-Taher, E.R. Shaaban, R. Elsaman, E. El Sayed Massoud, M.E. Mahmoud, *Nucl. Eng. Technol.* **54**, 2253 (2022).
- [5] M.A.K.A. Sttar, A.F. Mkhiaiber, A.M.A. Majeed, *AIP Conf. Proc.* **2190**, 020077 (2019).
- [6] M. Rashad, H.O. Tekin, H.M.H. Zakaly, M. Pyshkina, S.A.M. Issa, G. Susoy, *Nucl. Eng. Technol.* **52**, 2078 (2020).
- [7] B.C. Reddy, H.C. Manjunatha, Y.S. Vidya, K.N. Sridhar, U.M. Pasha, L. Seenappa, B. Sadashivamurthy, N. Dhananjaya, K.V. Sathish, P.S.D. Gupta, *Nucl. Eng. Technol.* **54**, 1062 (2022).
- [8] A. Saima, G. Henrika, L. Jouko, H. Simo-Pekka, *Nanoscale Res. Lett.* **13**, 179 (2018).
- [9] R.S. Khaleel, M.S. Hashim, *Kuwait J. Sci.* **47**, 1 (2020).
- [10] M.S. Hashim, R.S. Khaleel, *Surf. Interfaces* **20**, 100640 (2020).
- [11] M.S. Hashim, R.S. Khaleel, D.M. Naser, *Pak. J. Eng. Appl. Sci.* **29**, 58 (2021).
- [12] M.I. Sayyed, B. Albarzan, A.H. Almuqrin, A.M. El-Khatib, A. Kumar, D.I. Tishkevich, A.V. Trukhanov, M. Elsafi, *Materials* **14**, 3772 (2021).
- [13] S. Kaewjaeng, N. Chanthima, J. Thongdang, S. Reungsri, S. Kothan, J. Kaewkhao, *Mater. Today Proc.* **43**, 2544 (2021).
- [14] A.S. Mollah, *Bangladesh J. Nucl. Med.* **21**, 2 (2018).
- [15] M.I. Sayyed, A.H. Almuqrin, K.A. Mahmoud, A.S. Abouhaswa, *Sci. Rep.* **12**, 1800 (2022).
- [16] M.J.R. AL-Dhuhaihat, *Int. J. Appl. Innov. Eng. Manag.* **4**, 6 (2015).
- [17] A. Kumar, A. Jain, M.I. Sayyed, F. Laariedh, K.A. Mahmoud, J. Nebhen, M.U. Khandaker, M.R.I. Faruque, *Sci. Rep.* **11**, 7784 (2021).
- [18] E.E. Belgin, *Radiat. Phys. Chem.* **193**, 109960 (2022).